



Damage and Fragmentation of Rock Under Multi-Long-Hole Blasting with Large Empty Holes

Riyan Lan¹ · Ruishan Cheng² · Zilong Zhou³ · Lu Chen⁴ · Peiyu Wang³ · Zhen Wang³

Received: 12 November 2023 / Accepted: 28 April 2024
© The Author(s) 2024

Abstract

The technique of multi-long-hole blasting with large empty holes has been used in practice to break rock mass. However, the damage mechanism of rock mass surrounded by empty holes and boreholes under this type of blasting has not yet been well-understood and identified, which may lead to inappropriate design of the configurations of empty holes for multi-long-hole blasting. The present study investigates the damage modes and mechanism of rock mass under multi-long-hole blasting with large empty holes by conducting a field test and numerical simulations. The results show that multi-long-hole blasting with empty holes mainly causes compressive damage of rock mass around boreholes, reflected tensile damage near empty holes and ground surface, bending-induced tensile damage between empty holes and boreholes, shear damage along the side tangents and bottom of empty holes and boreholes, and tensile damage along the connection of boreholes caused by the superposition of stress waves. In addition, parametric studies are conducted to examine the effects of depths and diameters of empty holes and the spacing between boreholes and empty holes on the damage and fragmentation of rock mass under blast loads. It is found that the flexural stiffness and confined levels of rock mass can be greatly influenced by the variation of configurations of empty holes, which thus induces different damage and fragmentation under multi-long-hole blasting. Analytical formulas for the evaluation of shear and bending-induced damage of rock mass under multi-long-hole blasting are finally proposed to provide references for the design of empty holes in multi-long-hole blasting.

Highlights

- Damage modes and mechanisms of multi-long-hole blasting with large empty holes are identified.
- Rock fragmentation characteristics under this blasting are examined.
- Effects of configurations of empty holes on the performance of multi-long-hole blasting are revealed.
- Analytical formulas are developed to evaluate rock damage under this blasting.

Keywords Damage · Fragmentation · Long-hole blasting · Empty holes · Rock mass

Riyan Lan and Ruishan Cheng co-first authors: equal contribution.

✉ Ruishan Cheng
chengruishan@gmail.com

- ¹ Guangxi Xinfazhan Communication Group Co., Ltd., Nanjing, China
- ² Center for Infrastructural Monitoring and Protection, School of Civil and Mechanical Engineering, Curtin University, Perth, Australia
- ³ School of Resources and Safety Engineering, Central South University, Changsha, China
- ⁴ School of Civil Engineering, Changsha University of Science and Technology, Changsha, China

1 Introduction

The drill and blasting method has been popularly employed for ore extraction, engineering construction, and structural demolition due to its high efficiency and easy operation (Cheng et al. 2021a, b; Zhang et al. 2022, 2023). Highly confined blasting is often encountered in practice, e.g., the cut blasting for the excavation of tunnels (Shapiro 1989), drifts (AyalaCarcedo 2018), and shafts (Zhou et al. 2019). To ensure good blasting performance, empty holes are often drilled as potential relief space for highly confined blasting (Himanshu et al. 2021), since empty holes provide more

space to allow better expansion of blast-induced rock fragments and ensure effective throw of rock fragments from highly confined regions (Mandal et al. 2007). In addition, empty holes favor the reduction of borehole burdens due to reduced rock thickness around boreholes with the presence of free surfaces of empty holes (Konya and Walter 1991). However, drilling empty holes significantly increases work time and blasting costs due to additional drilling operations. Therefore, it is essential to finely design configurations of empty holes for highly confined blasting to minimize the losses caused by the drilling of empty holes.

To appropriately configure empty holes, many studies (Adhikari et al. 1999; Ding et al. 2023; Jong et al. 2004; Shi et al. 2023; Yilmaz 2023; Zare and Bruland 2006; Zhang et al. 2021) have investigated the configurations of empty holes on the performance of highly confined blasting. For example, Zhang et al. (2021) evaluated the crater forming performance induced by the cut blasting with a centric large-diameter empty hole. It was found that the spacing between empty holes and boreholes greatly affected the cut efficiency of rock craters. In addition, Shi et al. (2023) compared the rock damage induced by the nine-hole cut blasting with different layouts of empty holes. The results showed that the blast-induced rock damage depended to a large extent on the layout of empty holes around boreholes. Moreover, empty holes combined with long boreholes have been intensively used for large-scale blasting in practice to achieve high advance per round with less time cost. For instance, Liu et al. (2018) carried out the field test of two-shot long-hole raise blasting with multiple large-diameter empty holes to excavate a rock shaft with an axial length of 23 m. Another example given in Chandrakar et al. (2023) was that a 25 m length of rock shaft was advanced using single-shot long-hole blasting with multiple large-diameter empty holes. The results showed that high volume ratios of empty holes could facilitate the advancement of the blast-generated rock shaft. Due to the large volume of long-hole blasting in a single step, the fine requirements on the configurations of empty holes for long-hole blasting are further elevated as compared to those for short-advance blasting. Therefore, it is critical to appropriately configure empty holes for long-hole blasting to ensure effective advances and good fragmentation.

Currently, two methods based on expansion theory (Zare 2007) and empirical diagrams (Persson et al. 2018) are commonly used in practice to configure empty holes for long-hole blasting. The expansion theory specifies that the volume of rock fragments induced by blast loads is not greater than the total volume of empty holes, boreholes, and rock mass before blasting to allow the sufficient expansion of blast-induced rock fragments. The details on the expansion theory to design empty holes for long-hole blasting can be found in Zare (2007). It is noted that the expansion theory-based design assumes that the effective breakage of rock

mass between boreholes and empty holes can be achieved, which, however, needs to be calculated and validated. To ensure the effective breakage of rock mass between boreholes and empty holes, empirical diagrams given in Persson et al. (2018) are widely used in practice, among which the spacing of the borehole and empty hole is required less than 1.5 times the diameter of empty hole. However, the empirical diagrams-based design does not incorporate the effects of explosive properties, charge configurations, and rock conditions on the configurations of empty holes for long-hole blasting. Using the empirical diagrams to configure the empty holes for multi-long-hole blasting may cause poor breakage of rock mass and even failure to form effective rock damage between the boreholes and empty holes. Therefore, developing reliable design guidelines of empty holes for long-hole blasting is urgent to ensure effective damage and breakage of rock mass under long-hole blasting.

To provide a reliable design for long-hole blasting with empty holes, it is important to understand the damage modes and mechanism of rock mass surrounded by boreholes and empty holes. Currently, it is commonly agreed that the reduced burden around the boreholes due to the presence of empty holes can facilitate the blast-induced damage and breakage of rock mass between boreholes and empty holes (AyalaCarcedo 2018). However, to our best knowledge, the detailed damage modes and mechanism of the rock mass surrounded by empty holes and boreholes are not well-discussed and clarified yet. Therefore, this study aims to reveal the damage modes and mechanisms of rock mass under long-hole blasting with empty holes by a field test and numerical simulations. The effects of configurations of empty holes on blast-induced rock damage and fragmentation are also evaluated to better reveal the actions of empty holes on the performance of long-hole blasting. A discussion is finally conducted to propose analytical formulas for the evaluation of the damage of rock mass between boreholes and empty holes.

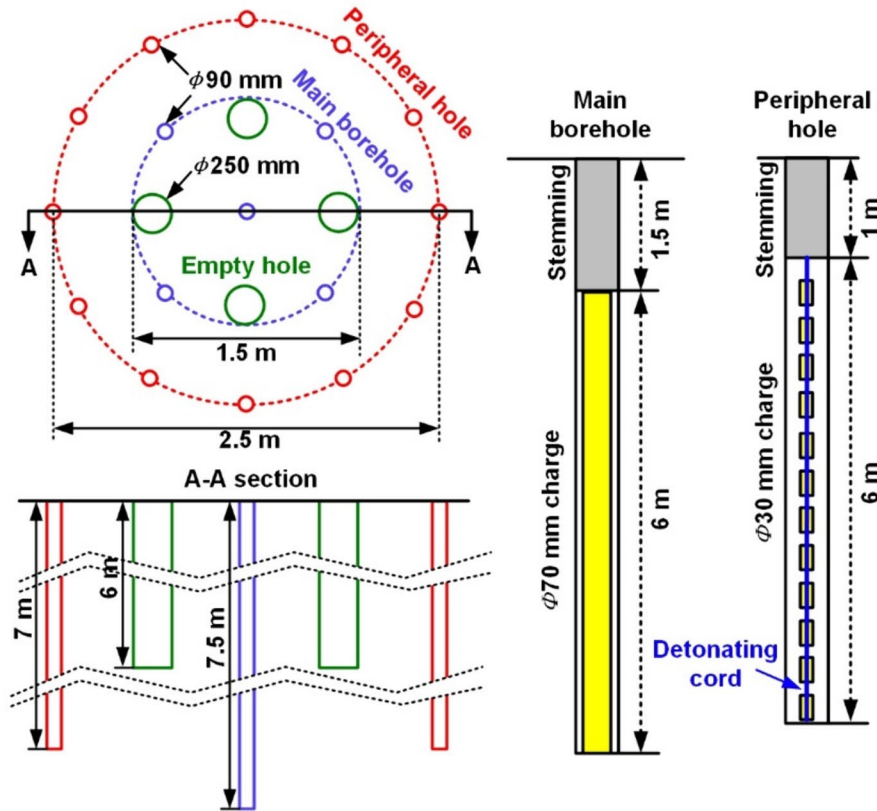
2 Field Test and Numerical Simulation

To investigate the damage and fragmentation of rock mass subjected to long-hole blasting with large-diameter empty holes, the field test and numerical simulation of a rock shaft excavated using the one-shot multi-long-hole blasting method are conducted in this section. The details are given below.

2.1 Test Setup

The field test for the blasting excavation of a rock shaft is carried out in an open-pit mine in China. The diameter of the rock shaft is expected to be 2.5 m. Figure 1a shows the

(a) Hole arrangement and charge structures



(b) Construction process

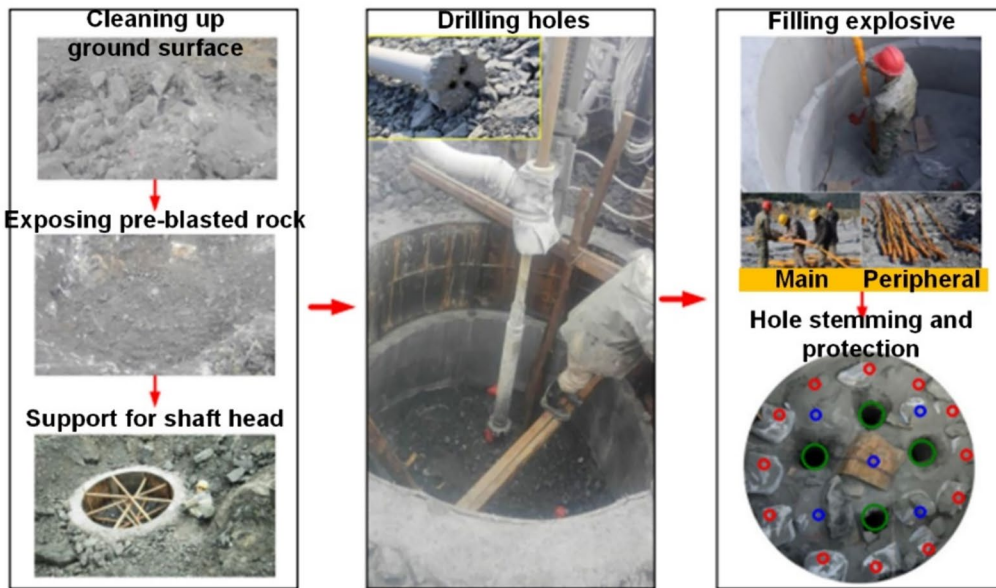


Fig. 1 Test setups of rock shaft using multi-long-hole blasting with large-diameter empty holes

details of hole arrangements for the blasting excavation of the rock shaft. A total of 12 peripheral holes with the same diameter of 90 mm are evenly assigned along the expected profile of the rock shaft. Five main boreholes along with

four empty holes are drilled inside the shaft boundary. The five main boreholes with the same diameter of 90 mm are arranged as a central borehole and four side boreholes evenly distributed along the circle at a distance of 0.75 m from the

central borehole. Four empty holes with the same diameter of 250 mm are arranged at equal angles around the central borehole and are inscribed with the circle across the four evenly distributed main boreholes. The designed depths of main boreholes, peripheral holes, and empty holes are 7.5 m, 6.5 m, and 5 m, respectively. However, the actual drilling depths of peripheral holes and empty holes are, respectively, 7 m and 6 m due to difficulties in controlling the drilling accuracy in the field test. The packaged emulsion explosive with a diameter of 70 mm is continuously filled in the main boreholes along the borehole depth. The peripheral holes are filled by a series of emulsion explosive columns, each 30 mm in diameter and 0.3 m in length. The axial gaps between adjacent explosive columns are set as 0.2 m. The detonating cord is used to connect different explosive columns in peripheral boreholes. The stemming lengths of the main and peripheral boreholes are 1.5 m and 1 m, respectively. Figure 1b shows the construction process to drill holes and fill charge. It is noted that the twelve peripheral boreholes are simultaneously detonated and are ignited 110 ms earlier than the main boreholes.

2.2 Numerical Models

Since it is difficult to record the entire process of rock blasting conducted in the field test, the numerical model of rock blasting with the same configurations as the field test is established in this section using LS-DYNA to reveal the damage process and mechanism of rock under long-hole blasting with large-diameter empty holes.

2.2.1 Finite-Element Model of Rock Shaft Blasting

Figure 2 shows the finite-element model of rock shaft blasting with multiple long boreholes and large-diameter empty holes, which keeps the same as the blasting design given in the field test. Since the blasting design given in Sect. 2.1 is symmetric along the centre of rock shaft, a quarter cylinder numerical model with a radius of 4 m and a height of 13 m is built in this section to save computational costs. The numerical model incorporates peripheral holes (two half peripheral holes and two full peripheral holes), main boreholes (a 1/4 centric hole and a full side hole), and empty holes (two half holes along the symmetric surfaces). The top surface of the model is specified as the free boundary to simulate the rock blasting with a single free surface. The right and left surfaces are assigned as symmetric boundaries to realize the assumption of model symmetry. Non-reflecting boundary is applied to the bottom and back surfaces of the numerical model to simulate the infinite domain of rock mass. The explosive is meshed using 50 mm solid elements, which is determined through mesh convergence study. To improve computational efficiency, the rock mass is meshed by gradually increased sizes of solid elements (50–200 mm) from close-in explosion areas to model boundaries. The gaps between the explosives and rock mass are filled by air layers, which share common nodes with explosives. To ensure effective transmission of explosion waves to surrounding rock mass, the air layers are partially overlapped with the rock mass. In addition, the arbitrary Lagrangian–Eulerian (ALE) multi-material

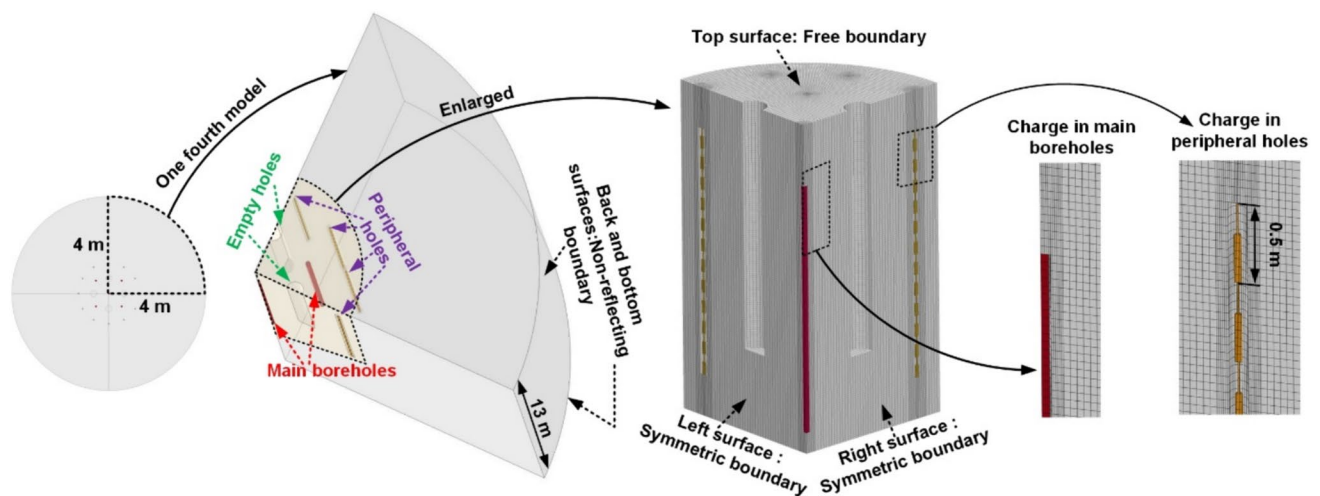


Fig. 2 Numerical model of multi-long-hole blasting with large-diameter empty holes

method combined with fluid–structure–interaction (FSI) approach is employed to achieve the interaction between rock mass and explosive. The stemming and charge structures of main boreholes and peripheral holes keep the same as those given in the field test.

2.2.2 Material Models and EOS

Rock mass, explosive, and air are presented in the numerical models. In this study, *MAT_RHT, *MAT_HIGH_EXPLOSIVE_BURN, and *MAT_NULL are employed as the material models of rock mass, explosive, and air, respectively. A total of 37 parameters (see Table 1) are required for *MAT_RHT to simulate the behaviour of rock mass under blast loads. The basic parameters are determined based on the mechanical properties of rock mass in the field test. The parameters significantly influencing the behaviour of *MAT_RHT (e.g., failure surface parameters) are obtained by empirical equations given in Liu et al. (2018). The accuracy of those empirical equations in determining corresponding parameters has been widely evaluated and validated in existing studies (Liu et al. 2018; Xie et al. 2017; Li et al. 2022), which are thus employed in this study. The remaining parameters are integrated from Xie et al. (2017) and Liu et al. (2018).

To simulate the pressure of explosive detonation, Jones–Wilkins–Lee (JWL) equation of state (EOS) is employed. In addition, *EOS_LINEAR_POLYNOMIAL

is utilized to describe the pressure states of air. The parameters of material models and equation of state (EOS) for explosive and air are given in Table 2.

2.3 Comparison of Test and Simulation Results

2.3.1 Comparison of Shaft-Forming Results and Simulated Damage

Figure 3 shows the measured results of blast-generated rock shaft and the profiles of simulated blast-induced rock damage. The overall depth of the rock shaft formed in the test is approximately 6.2 m. An obvious overbreak area on the upper left side of the rock shaft along the cross section is observed, which may be caused by the combined actions of blast loads and macro-cracks at the area. However, no obvious overbreak is formed in the simulation, since no macro-crack is incorporated in the numerical model due to the difficulties in determining the features of actual macro-cracks. Meanwhile, it can be found that when the depth of the rock shaft is not greater than 5.3 m, the simulated damage profile with the damage levels over 0.8 (i.e., red area) can well-agree with the measured profile of the rock shaft along the cross section (see B–B section). Moreover, the rock mass in the main blasting area with the shaft depths between 5.3 and 6.2 m is still well-broken in the test. However, the rock mass between the main blasting areas and peripheral holes in the same depth ranges is not effectively

Table 1 Parameters of RHT model (Liu et al. 2018; Xie et al. 2017) for rock mass used in this study

Type	Specific parameter	Value	Specific parameter	Value
Basic parameters	Tensile strength (MPa)	9	Elastic shear modulus (GPa)	13.27
	Shear strength (MPa)	72	Density (kg/m ³)	2518
	Compressive strength (MPa)	90		
Strain rate parameters	Reference compressive strain rate E_{0c}	$3e^{-5}$	Reference tensile strain rate E_{0t}	$3e^{-6}$
	Break compressive strain rate E_c	$3e^{25}$	Break tensile strain rate E_t	$3e^{25}$
	Tensile strain rate dependence exponent	0.0182	Compressive strain rate dependence exponent	0.0138
Strength parameters	Lode angle dependence factor Q_0	0.68	Lode angle dependence factor B	0.05
	Compressive yield surface parameter G_c	0.53	Tensile yield surface parameter G_t	0.7
	Volumetric plastic strain fraction in tension P_{tf}	0.001	Erosion plastic strain E_{psf}	2
	Shear modulus reduction factor X_f	0.8	Minimum damaged residual strain E_{pm}	0.015
	Residual surface parameter A_f	0.25	Residual surface parameter N_f	0.62
	N : failure surface parameter	0.68	A : failure surface parameter	2.65
Damage parameters	Damage parameter D_1	0.04	Damage parameter D_2	1
EOS parameters	Initial porosity α_0	1.0	Porosity exponent N_p	3
	Gruneisen gamma γ	0	Compaction pressure P_{co} (GPa)	6
	Parameter for polynomial EOS B_0	1.22	Parameter for polynomial EOS B_1	1.22
	Parameter for polynomial EOS T_1 (GPa)	36.22	Parameter for polynomial EOS T_2	0
	Crush pressure (MPa)	60	A_1 : Hugoniot polynomial coefficient (GPa)	13.27
	A_2 : Hugoniot polynomial coefficient (GPa)	19.50	A_3 : Hugoniot polynomial coefficient (GPa)	8.50

Tensile and compressive strain rate dependence exponents, A , N , A_1 , A_2 , A_3 , and crush pressure are determined based on empirical equations given in Liu et al. (2018)

Table 2 Material models and EOS of emulsion explosive and air and corresponding parameters

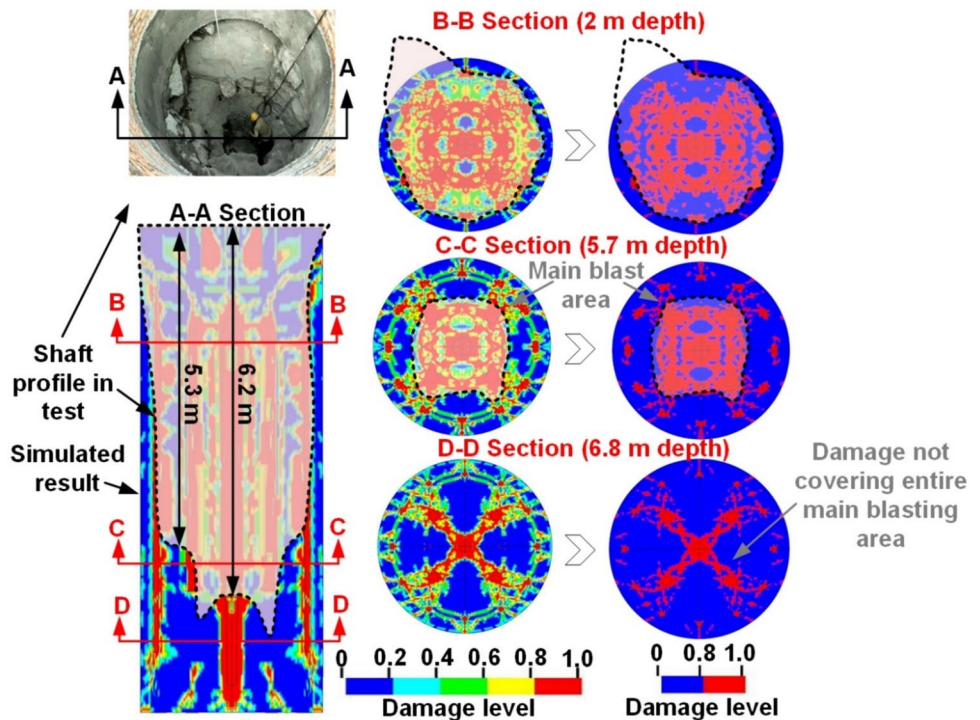
Component	Material model and EOS	Parameter	Value
Emulsion explosive (Sanchi-drian et al. 2015)	*MAT_HIGH_EXPLOSIVE_BURN *EOS_JWL $P = A \left(1 - \frac{\omega}{R_1 V} \right) e^{R_1 V} + B \left(1 - \frac{\omega}{R_2 V} \right) e^{R_2 V} + \frac{\omega E}{V}$	Density (kg/m ³)	1260
		Detonation velocity (m/s)	5270
		Chapman–Jouget pressure (GPa)	8.127
		Constant A (GPa)	557.6
		Constant B (GPa)	5.349
		Constant R ₁	6.1
		Constant R ₂	1.072
		Constant ω	0.24
		Initial internal energy E ₀ (J/m ³)	4 × 10 ⁹
		Air	*MAT_NULL *EOS_LINEAR_POLYNOMIAL $P = C_0 + C_1 \mu + C_2 \mu^2 + C_3 \mu^3 + (C_4 + C_5 \mu + C_6 \mu^2) E_r$
		Constants C ₀ , C ₁ , C ₂ , C ₃ , C ₆	0
		Constants C ₄ , C ₅	0.4
		Initial internal energy E _{r0} (J/m ³)	2.5 × 10 ⁵

P, *V*, *E* and *μ* are hydrostatic pressure, relative volume, internal energy of explosive per unit volume, and compression parameter, respectively. The height of test site is not greater than 50 m above sea level and thus the density of air at sea level (i.e., 1.255 kg/m³) is used in this study

broken in the test due to the intensive rock constraints around the shaft bottom. Similarly, in this simulation, the rock mass in the main blasting area with the same depth ranges as the test is sufficiently damaged (see C–C section), while no effective damage (i.e., the damage levels over 0.8) is formed between the main blasting area and peripheral holes in the same depth ranges. In addition, the main blasting area with the rock depths over 6.2 m is not effectively damaged in the simulation (see D–D section

of Fig. 3), despite the damage over 0.8 along the connection of the centric borehole and four side boreholes is observed. In the test, the rock mass over the depth of 6.2 m is not well-fractured and cannot be removed, thus forming the rock shaft with the depth around 6.2 m. That is to say, the damage in the rock mass with the depths of more than 6.2 m is visually visible in the simulation, while no effective failure in the same depths of rock mass is formed in the test. This is because the rock constraints caused by

Fig. 3 Blast-generate profile of rock shaft in the test and simulated damage profile



the volume expansion with the rock fragmentation are not able to be incorporated in the simulation. Based on the above results, it can be concluded that the simulated damage with the damage level over 0.8 has good agreements with the measured blast-generated rock shaft profile. The intensive rock constraints around the bottom of rock shaft are prone to prohibit the damage and fragmentation of rock mass under blast loads. It should be pointed out that to better conform with the test results, the simulated damage in the main blasting area should be considered invalid once the damage does not cover the entire main blasting area. In addition, difference in blast-induced rock damage along the horizontal and vertical directions observed from the top view may be attributed to non-perfectly symmetrical mesh configurations in the quarter model. That is, the elements divided in the quarter model are not symmetrically distributed exactly along the angular bisector of the quarter model from the top view. However, the simulated damage of rock mass is overall acceptable by comparing it with the test results, which indicates the accuracy of the established model in analyzing the performance of multi-long-hole blasting with large empty holes.

2.3.2 Comparison of Rock Fragmentation

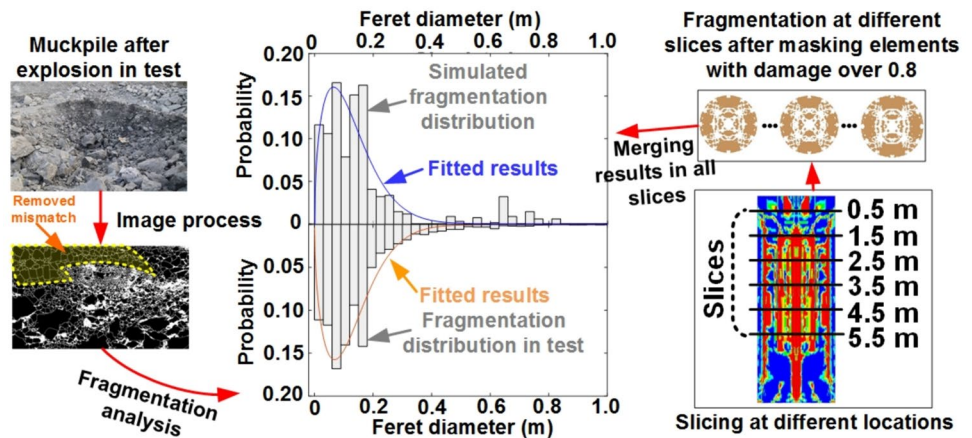
In addition to the shaft-forming results, the fragmentation level of rock mass is greatly concerned by designers and engineers, since the fragment sizes significantly affect the efficiency of fragment removal from the shaft. Many indicators, such as maximum and mean lengths (Hudaverdi et al. 2012) of fragments and equivalent spherical diameter (Roy et al. 2016; Sanchidrián et al. 2007) can be employed to represent fragment sizes. The equivalent spherical diameter characterized by Feret diameter (defined as the fragment perimeter divided by π) is used in this study, since the indicator considers the irregularity of morphology of broken fragments. In addition, two indicators, i.e., the weight (Thurley 2011) and the number (Li et al. 2022) of different sizes of fragments are often employed to reveal the size distribution characteristics of fragments. In this section, the number of fragments with various sizes is employed to evaluate the size distribution of fragments, since the indicator is easy to obtain using the ImageJ code. Moreover, many empirical equations to predict the size distribution of blast-induced rock fragments have been proposed by assuming distribution functions, as reviewed by Ouchterlony and Sanchidrián (2019). The Weibull distribution function is the popular one of them and is employed in this study. Its probability density function f is defined as

$$f(x) = n \left(\frac{x}{x_c} \right)^{m-1} \exp \left(- \left(\frac{x}{x_c} \right)^m \right), \quad (1)$$

where x is the fragment size, i.e., Feret diameter in this study. x_c is the scale parameter and m is the shape parameter. n is obtained based on x_c and m .

To investigate the characteristics of rock fragmentation induced by multi-long-hole blasting with large-diameter empty holes, the muckpile of broken rock mass around the rock shaft in the test is processed by using the image processing code ImageJ and the results are analyzed and discussed in this section. In addition, the blast-induced rock fragmentation in the numerical simulation is obtained by masking the rock mass over a certain level of damage (i.e., the excessive crushing rock). This approach has been widely used and proved to be reliable in existing studies (Li et al. 2022). The damage threshold in the simulation is determined as 0.8 by multiple trials (i.e., by comparing the test results with the simulated results obtained sequentially by varying the thresholds from 0.5 to 0.9). To accurately obtain the size distribution characteristics of blast-induced rock fragments in the numerical simulation, multiple slices (i.e., 6 slices with the same interval of 1 m) along the depths of rock shaft are obtained and processed using the ImageJ code. The analysis results of rock fragmentation in different slices are combined to represent the overall fragmentation characteristics. It is noted that multiple photos documenting blast-induced rock fragmentation from different views are taken in the field test. The best one effectively and maximumly capturing the fragment muckpile is adopted and processed using the ImageJ code. To ensure the accuracy of rock fragmentation identified by the ImageJ, different methods in ImageJ are employed to analyze the original photo for the generation of rock fragmentation. A grey image visually showing the optimal match of rock fragments with the real results in the original photo is generated using the watershed method given in ImageJ. In addition, the mismatched rock fragments between the processed image and the original photo are manually removed by carefully comparing the difference between two pictures (see Fig. 4) before conducting fragmentation analysis, which thereby further ensures accurate and comprehensive presentation of rock fragmentation. Figure 4 shows the size distributions of blast-induced rock fragments in the test and numerical simulation. It can be found that both measured and simulated fragment sizes mainly concentrate in the size range less than 0.4 m. More specifically, the proportion of fragments with the sizes between 0.06 m and 0.2 m is much high. In addition, the fitted results based on Eq. (1) agree with the fragmentation obtained from the test and simulation. The results show the blast-induced rock fragment distribution can be

Fig. 4 Size distributions of blast-induced rock fragments in the test and simulation



well-characterized by the Weibull distribution function. Moreover, good matches of fitted results between the test and simulation are achieved. For instance, the scale parameter and shape parameter of the Weibull distribution function in the test are, respectively, 0.138 and 1.52, which are very close to those (i.e., 0.137 and 1.48) in the simulation. The above results show the rock fragmentation induced by the multi-hole-blasting can be well-predicted using the Weibull distribution function. It is also reliable to characterize the size distribution of fragments in the simulation by masking the rock mass with the damage over 0.8.

3 Damage and Fragmentation Analysis

The comparison given in Sect. 2.3 reveals the numerical model established in this study is able to accurately predict the response of rock mass subjected to multi-long-hole blasting. Therefore, the numerical simulation is further used to analyze the damage process and mechanism of rock mass under multi-long-hole blasting with large-diameter empty holes. The details are given below.

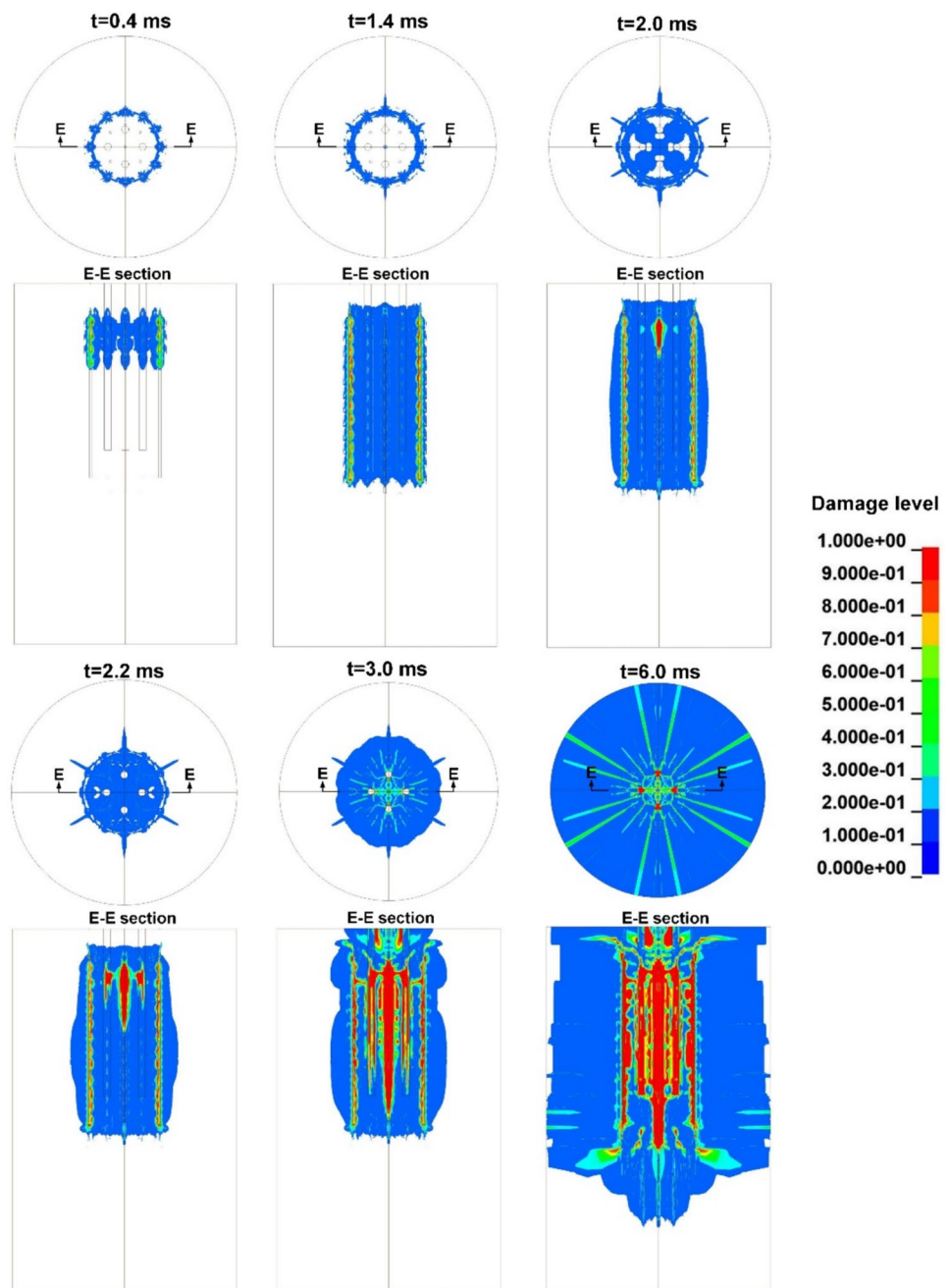
3.1 Damage Mode and Mechanism

Figure 5 shows the damage process of rock mass under multi-long-hole blasting with large-diameter empty holes. The charge at the top of peripheral holes is first ignited. At the time instant of 0.4 ms, the explosive in the peripheral holes has been fully detonated and the rock damage along the cross-sectional profile of rock shaft is generated from the top to the bottom of peripheral holes. The main boreholes start ignition at 2 ms, immediately followed by the severe damage (i.e., red area) of rock mass around the detonated charge in the main boreholes. In addition, the rock damage around empty holes occurs at 2.2 ms. With the continuous detonation of charge in the main boreholes, the damage around the main boreholes and empty holes are further

intensified. The rock damage near the ground surface of rock mass is also generated at 3 ms with stress waves arriving at the ground surface. The final rock damage is presented at 6 ms with the aggregation and connection of different types of damage.

To clearly reveal the damage mechanism of rock mass under multi-long-hole blasting with large-diameter empty holes, the damage states of rock mass subjected to blast loads at different time instants are further analyzed, as shown in Fig. 6. The main borehole blasting begins at 2 ms and the compressive damage of rock mass around the detonated charge in main boreholes is immediately presented under intensive blast pressure. As the time increases to 2.2 ms, severe damage around empty holes is formed although the slight deformation around empty holes is observed (see the enlarged view at 2.2 ms). It is because the surface of empty holes induces significant reflections of blast-induced stress waves arriving at empty holes, which thus leads to intensive tensile failure of rock mass around empty holes. The slight deformation near empty holes causes slight shear damage of rock mass between empty holes and main boreholes due to the uncoordinated deformation of rock mass around the shear damage. In addition, the shear damage of rock mass between main boreholes and peripheral holes is generated at 2.2 ms (see O–O section and P–P section), which is because the expanded peripheral holes induced by peripheral hole blasting is easy to cause the stress concentration of rock mass between main boreholes and peripheral holes under the main borehole blasting. Meanwhile, the tensile damage along the connections of different main boreholes is generated due to the superposition of stress waves from different main borehole blasting (see O–O section at 2.2 ms). With the time increased to 3 ms, the shear damage between main boreholes and empty holes as well as main boreholes and peripheral holes is further increased due to further increased uncoordinated deformation of rock mass. The tensile damage of rock mass along the connections of

Fig. 5 Damage process of rock mass under multi-long-hole blasting with large empty holes



different main boreholes is also increased with the further propagation and interaction of blast waves. In addition, the bending deformation of rock mass between main boreholes and empty holes is induced under the main borehole blasting (see the enlarged view at 3 ms), which aggravates the tensile damage of rock mass at corresponding locations. As the time comes to 6 ms, different types of damage are connected and clustered to form final rock damage. It is noted that the damage between main boreholes and peripheral holes is further increased due to (1) the increase of shear damage and (2) tensile damage induced by the rock deformations towards the empty holes. It is also found

that the rock damage near the ground surface and the top of empty holes is generated at 3 ms and is continuously aggravated until 6 ms, which is caused by the combined reflection of stress waves at the ground surface and empty holes. Based on the above results, it can be concluded that the rock mass under multi-long-hole blasting with large empty holes experiences different types of damage involving compressive damage around boreholes, tensile damage near empty holes and ground surface, bending-induced tensile damage between empty holes and boreholes, shear damage along the side tangents and bottom of empty holes and boreholes, and tensile damage along the connection of

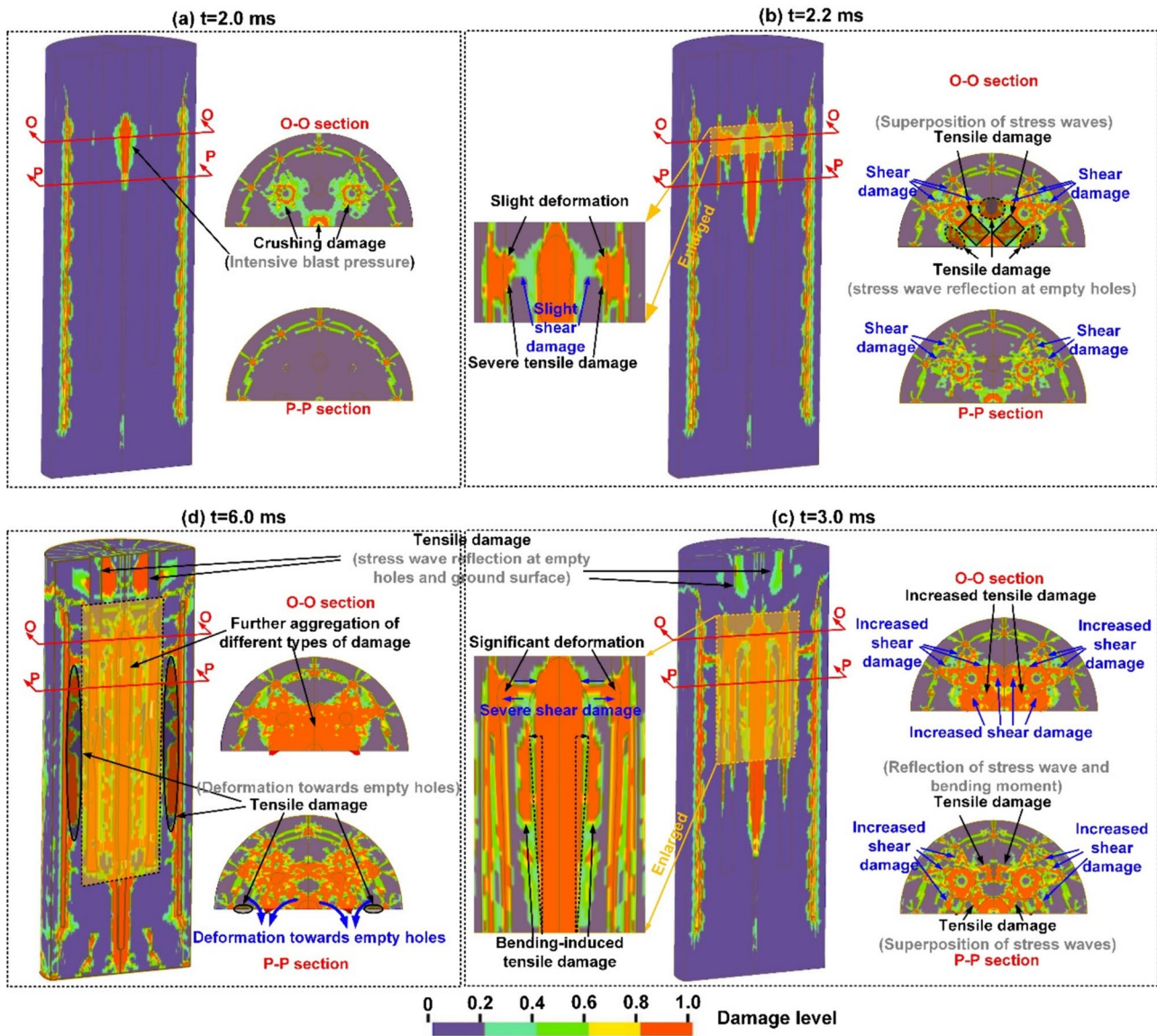


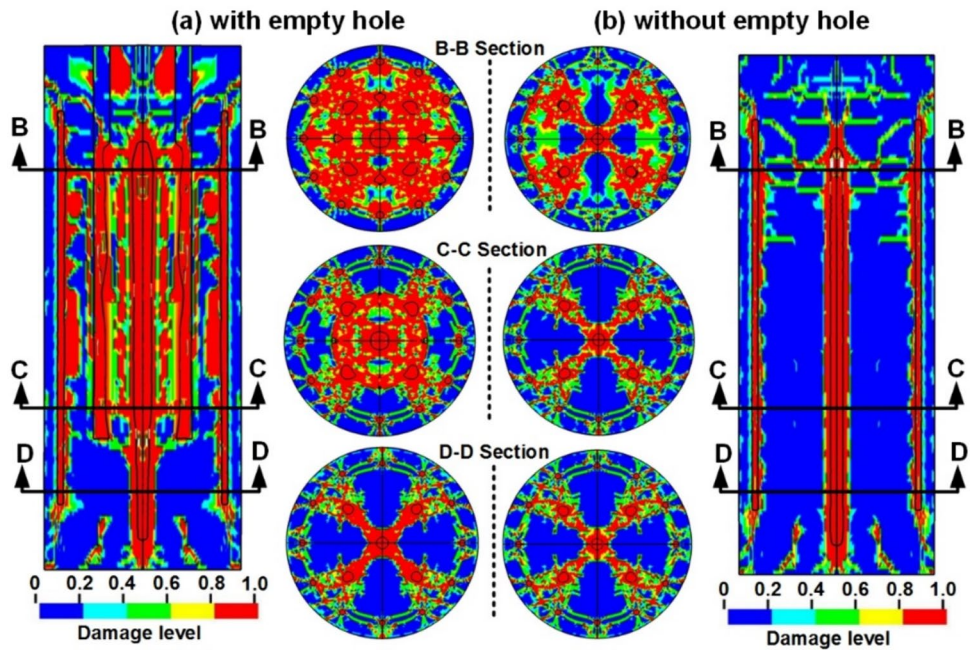
Fig. 6 Damage modes of rock mass at different time instants under multi-long-hole blasting with large empty holes. Deformations in partial figures is enlarged to five times for illustration

boreholes caused by the superposition of stress waves. The empty holes significantly affect the generation, connection, and aggregation of rock damage under blast loads.

To reveal the effects of empty holes on the performance of multi-long-hole blasting, the damage difference of rock mass under multi-long-hole blasting with and without large-diameter empty holes is discussed and compared. Figure 7 shows the damage of rock mass under the two types of multi-long-hole blasting. It can be seen that the damage of rock mass in the case with empty holes is significantly higher than that without empty hole. The rock damage in the main blasting area as well as the area between the main boreholes and peripheral holes is effectively connected and aggregated in the case with empty holes (see the vertical view

in Fig. 7a). However, the damage of rock mass in the case without empty hole mainly concentrates on the area around the main boreholes and peripheral holes (see the vertical view in Fig. 7b). In addition, according to different cross-sectional views, it can be found that at relatively shallow depths (e.g., B–B section), effective rock damage can cover the entire cross-sectional area in the profile of the rock shaft in the case with empty holes, while rock damage in the case without empty hole is mainly presented at the connection area of different main boreholes as well as the area between four side main boreholes and adjacent peripheral holes. The damage of rock mass in the area between adjacent side main boreholes is not observed in the case without empty hole. As the depth of rock mass increases, the damage ranges in the

Fig. 7 Final damage of rock mass under multi-long-hole blasting with and without empty holes



cases with and without empty holes both gradually reduce. However, the rock damage can still cover the entire main blasting area in the case with empty holes with the depth increasing to the bottom of empty holes (see C–C section in Fig. 7). As the depth of rock mass exceeds the bottom of empty holes, the rock damage cannot completely encompass the main blasting area in the case with empty holes and has similar distributions with that in the case without empty holes (see D–D section in Fig. 7). Moreover, it can be seen that the rock damage near the ground surface in the case with empty holes is obviously more severe than that without

empty holes due to the combined reflection actions of empty holes and ground surface on blast-induced stress waves.

The presence of empty holes can contribute to the tensile damage of rock mass near the empty holes (see Fig. 6b) due to the reflection of surface of empty holes on blast-induced stress waves. In addition, the empty holes reduce the flexural stiffness of rock mass in main blasting areas due to the reduced rock thickness between main boreholes and empty holes, which is beneficial to deform the rock mass under bending moments induced by blast loads. The empty holes also provide more space to accommodate the deformed rock mass, which enables more blast-induced deformation

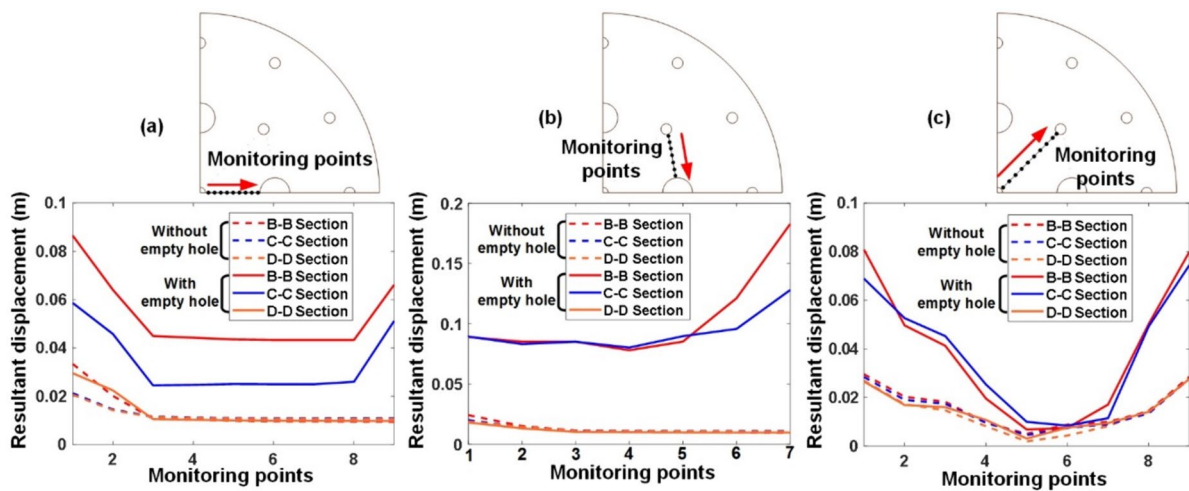


Fig. 8 Blast-induced peak resultant displacements along the connections of **a** the centric main borehole and empty holes, **b** the side main borehole and empty holes, and **c** the centric and side main boreholes in the cases with and without empty holes

of rock mass in the case with empty holes and thus causes more severe damage of rock mass than that without empty hole. As shown in Fig. 8a, b, the peak resultant displacements between main boreholes and empty holes in the case with empty holes are significantly higher than those without empty holes. For instance, at the connection of the central main borehole and empty hole (see Fig. 8a), the peak resultant displacements at all monitoring points in the case with empty holes are at least 0.04 m greater than those at the same monitoring points in the case without empty holes. Moreover, compared to the relatively far area from the empty hole along these connections, the deformation of rock mass around the empty holes can be more obviously increased, since the rock mass around empty holes experiences less constraints from surrounding rock mass. It is worth mentioning that the deformation of rock mass along the connection of the central main borehole and side main boreholes is also increased as compared to those without empty holes. The increased deformation of rock mass is more obvious near the main boreholes while gradually becoming less significant from the main boreholes to the centre of their connection, which indicates the rock mass around the main boreholes along the connection is easier to deform towards the empty holes. In summary, the empty holes can significantly increase the blast-induced deformation of rock mass in main blasting areas, which thus favors the damage of rock mass under blast loads.

3.2 Rock Fragmentation Evaluation

In addition to the blast-induced damage range of rock mass, rock fragmentation is an important indicator to evaluate the blasting performance. The overall size distribution characteristics of rock fragments induced by the multi-long-hole blasting with empty holes are discussed in Sect. 2.3.2. To reveal the contribution of rock fragments at different rock depths to the overall distribution of fragmentation, Fig. 9a shows the ratios of different sizes of rock fragments in multiple cross sections with different sizes rock depths. It can be

found that at relatively shallow rock depths (e.g., 0.5 m), rock fragments with large sizes (e.g., greater than 0.6 m) take up much higher ratios, which implies that the top of the blasting area is prone to form rock boulder. It is because no explosive is filled at the relatively shallow depths and thus less intensive blast waves act on the rock mass at corresponding depths. As the rock depth increases to 1.5 m, the ratios of rock fragments with sizes greater than 0.6 m drastically decrease and keep basically stable with the rock depths increasing from 3.5 to 5.5 m. In addition, Fig. 9b shows the median sizes of blast-induced rock fragments at different rock depths. It can be seen that the median sizes of rock fragments first significantly reduce and then keep basically stable with the rock depths increasing from 0.5 to 5.5 m, which reveals that the constraints of rock mass at the relatively large depths to the rock mass in blasting areas are effectively reduced. In summary, the presence of empty holes enables the effective release of constraints to rock mass in main blasting areas and facilitates the breakage levels of rock mass.

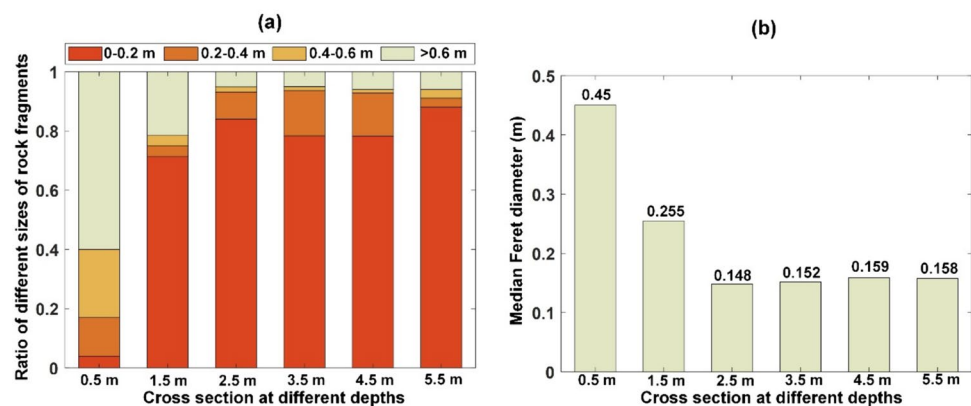
4 Parametric Study

As discussed above, the empty holes can significantly affect the levels of damage and fragmentation of rock mass under multi-long-hole blasting. To investigate the effects of the configurations of empty holes on the damage and fragmentation of rock mass under multi-long-hole blasting, the numerical models of rock mass subjected to the multi-long-hole blasting with different characteristics of empty holes (i.e., different depths and diameters of empty holes, and different spacings of centric main boreholes and empty holes) are established. The details are given below.

4.1 Effects of Depth of Empty Hole

To investigate the effect of depths of empty holes on the damage and fragmentation of rock mass under the

Fig. 9 Characteristics of blast-induced rock fragments. **a** Ratios of different sizes of rock fragments at multiple cross sections, **b** median size of rock fragments at multiple cross sections



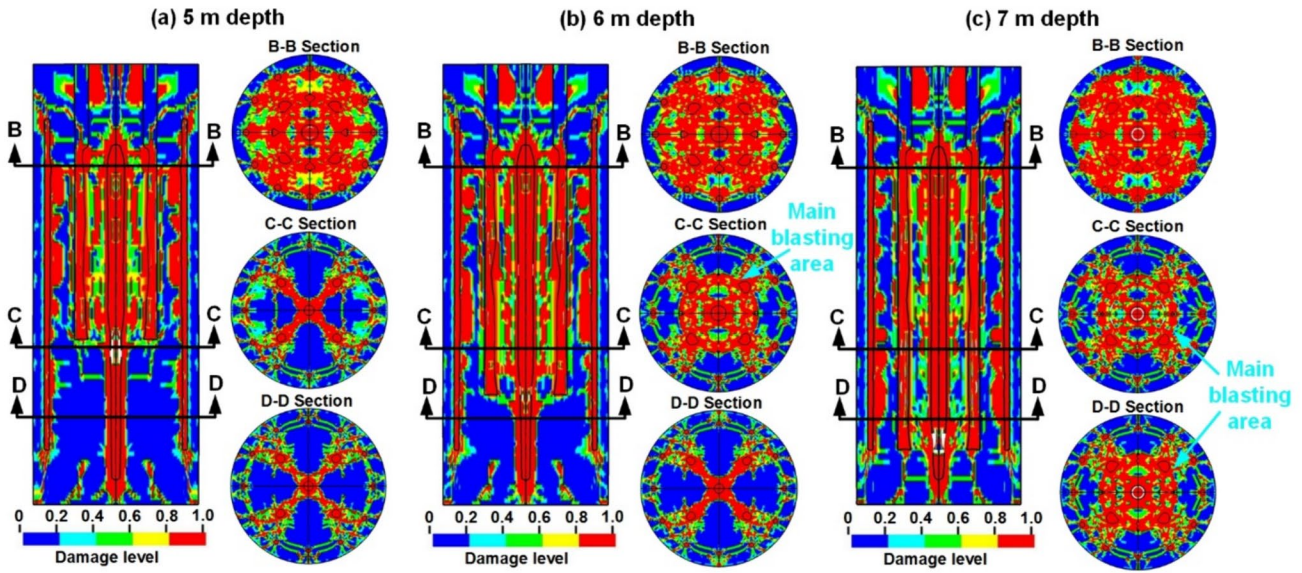


Fig. 10 Final damage of rock mass under multi-long-hole blasting with different depths of large empty holes

multi-long-hole blasting, the numerical models of rock mass under the multi-long-hole blasting with 5 m, 6 m, and 7 m depths of empty holes are, respectively, built in this section. Besides the depths of empty holes, other configurations of these three numerical models keep the same as those given in Sect. 2.2.

Figure 10 shows the final damage of rock mass subjected to multi-long-hole blasting loads in the cases with different depths of empty holes. It can be found that the effective damage depths of rock mass are greatly dependent on the depths of empty holes. For instance, the effective damage depth of rock mass in the case with 5 m deep empty holes is approximately 5 m (see vertical view of

Fig. 10a). The effective rock damage cannot cover the entire main blasting area with the depth of rock mass over 5 m, as shown in cross-sectional views (i.e., C–C section and D–D section) of Fig. 10a. However, the effective damage depths of rock mass in the cases with 6 m and 7 m empty holes can approximately reach 6 m and 7 m, respectively. As shown in Fig. 10b, effective damage (i.e., red area) of rock mass can encompass the main blasting area in the C–C section but cannot cover the main blasting area in the D–D section in the case with 6 m deep empty holes. In addition, the effective damage of rock mass in the case with 7 m deep empty holes can cover the main blasting areas in both the C–C section and D–D section.

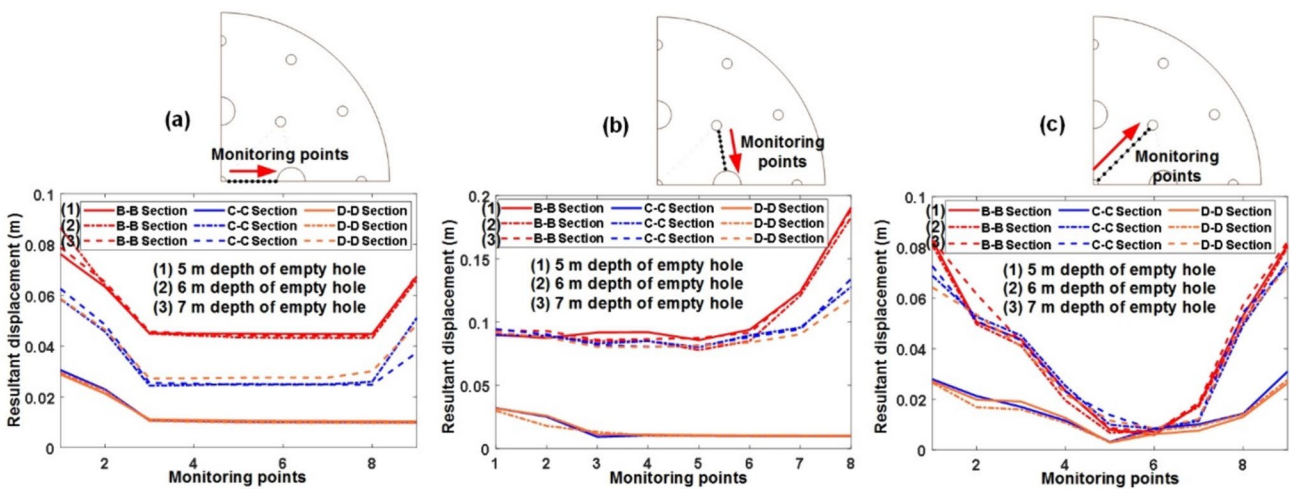


Fig. 11 Blast-induced peak resultant displacements along the connections of a the centric main borehole and empty holes, b the side main borehole and empty holes, and c the centric and side main boreholes in the cases with different depths of empty holes

Therefore, it can be concluded that the depths of empty holes significantly influence the depth of effective damage of rock mass (i.e., the effective shaft-forming depth) under the multi-long-hole blasting.

The significant actions of depths of empty holes on the damage depths of rock mass under the multi-long-hole blasting is due to the fact that the blast-induced rock deformation in main blasting areas is greatly affected by the presence of empty holes. Figure 11 shows the peak resultant displacements along the connections between main boreholes and empty holes as well as the connection between the centric main borehole and side main boreholes in three cross sections with different rock depths (i.e., B–B section, C–C

section, and D–D section). It can be seen from Fig. 11a, b that the displacements along the connections of main boreholes and empty holes in the cross sections containing empty holes are obviously higher than those in the cross sections without empty holes. For instance, the displacements along the connection of the centric main borehole and empty hole in the C–C section (see Fig. 11a) in the case with 5 m deep empty holes is significantly lower than those in the C–C section in the cases with 6 m and 7 m deep empty holes. It is because the empty holes are not included in the C–C section in the case with 5 m deep empty holes, but are still included in the section in the cases with 6 m and 7 m deep empty holes. In addition, it is found from Fig. 11c that the deformation along the connection of the centric main borehole and side main boreholes, especially near the main boreholes, is also significantly increased by the empty holes. For instance, the displacements around the main boreholes along the connection of the centric main borehole and side main boreholes in the D–D section in the cases with 5 m and 6 m deep empty holes are significantly lower than those in the D–D section in the case with 7 m deep empty holes.

To investigate the effect of depths of empty holes on the fragmentation of rock mass under the multi-long-hole blasting, the overall size distributions of blast-induced rock fragments in the above three cases are obtained (see Fig. 12) by combining the analysis results of rock fragment sizes in multiple cross-sectional slices with different rock depths. It is noted that the deepest cross-sectional slice in each case is above the bottom of the effective formed shaft (i.e., the lowermost depth with the rock damage effectively covering entire cross-sectional main blasting areas). The fitted results of size distributions of rock fragments based on Eq. (1) for

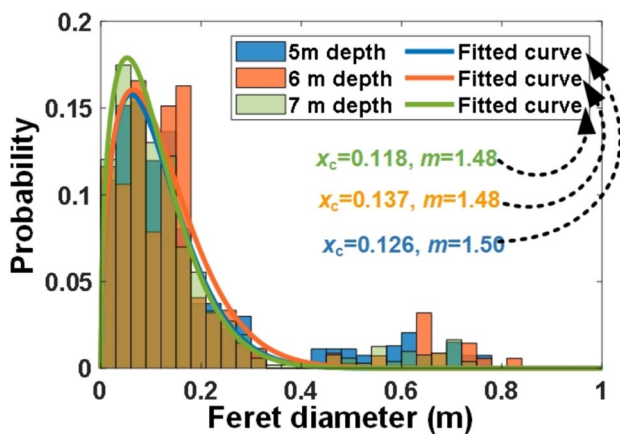


Fig. 12 Size distributions of blast-induced rock fragments in the cases with different depths of empty holes. Brown bars are the overlapping results of yellow and blue bars (Color figure online)

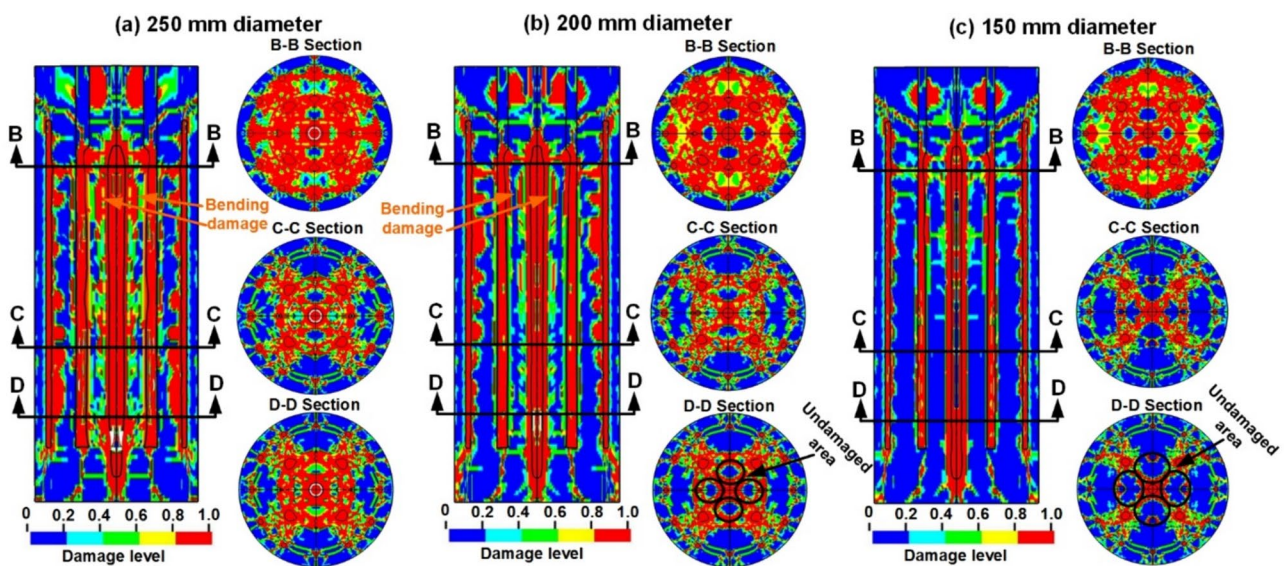


Fig. 13 Final damage of rock mass under multi-long-hole blasting with different diameters of large empty holes with a same depth of 7 m

these three cases are also given in Fig. 12. It can be seen that the blast-induced rock fragments in the cases with 5 m and 6 m deep empty holes have very similar distribution characteristics. With the depth of empty holes increased to 7 m, the probability of small sizes of rock fragments is increased. The results indicate that increasing the depth of empty holes beyond a certain level (e.g., 7 m in this study) can generate more small sizes of rock fragments under the multi-long-hole blasting with empty holes.

4.2 Effects of Diameter of Empty Hole

To investigate the effect of diameters of empty holes on the performance of multi-long-hole blasting, the numerical models of rock mass under the multi-long-hole blasting with three different diameters (i.e., 250 mm, 200 mm, and 150 mm) of empty holes are, respectively, built in this section. Besides, other configurations of numerical models remain the same as those in Sect. 2.2.

Figure 13 shows the final damage of rock mass subjected to these three forms of multi-long-hole blasting loads. The vertical view of Fig. 13 shows that the damage is significantly reduced with the decreased diameters of empty holes. Specifically, the damage between main boreholes and empty holes is decreased with the diameter of empty holes decreased from 250 to 150 mm. It is because the bending deformation of rock mass between main boreholes and empty holes can be obviously reduced due to the increased thickness of corresponding rock mass with the decreased diameters of empty holes. As shown in the D–D sections of Fig. 13, the rock mass between the centric main borehole and empty holes is almost completely damaged (i.e., red area) in the case with 250 mm diameter of empty holes, while the partial rock mass between the centric main borehole and

empty holes is not damaged (i.e., blue area) in the case with 200 mm diameter of empty holes and the undamaged area is further increased in the case with 150 mm diameter of empty holes. The above results indicate that the diameter of empty holes can significantly influence the effective damage of rock mass under multi-long-hole blasting.

Figure 14 shows the deformation of rock mass in main blasting areas in multiple cross sections (B–B section, C–C section, and D–D section) with different rock depths. It can be seen that the diameters of empty holes can obviously affect the deformation of rock mass in the main blasting areas. For instance, the peak resultant displacements of rock mass along the connection of the centric main blasting borehole and empty holes in the B–B section is higher in the case with larger diameter of empty holes. In addition, it can

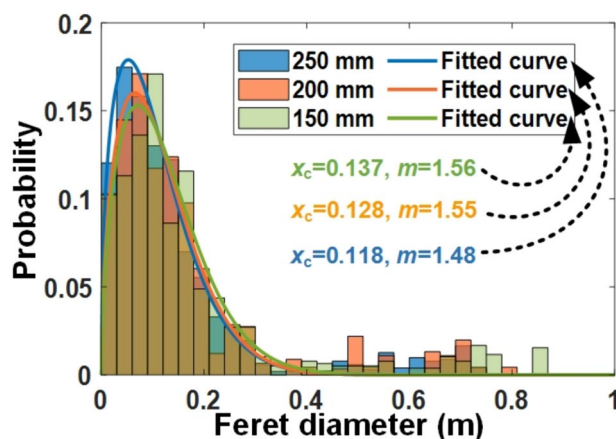


Fig. 15 Size distributions of blast-induced rock fragments in the cases with different diameters of empty holes. Brown bars are the overlapping results of yellow and blue bars (Color figure online)

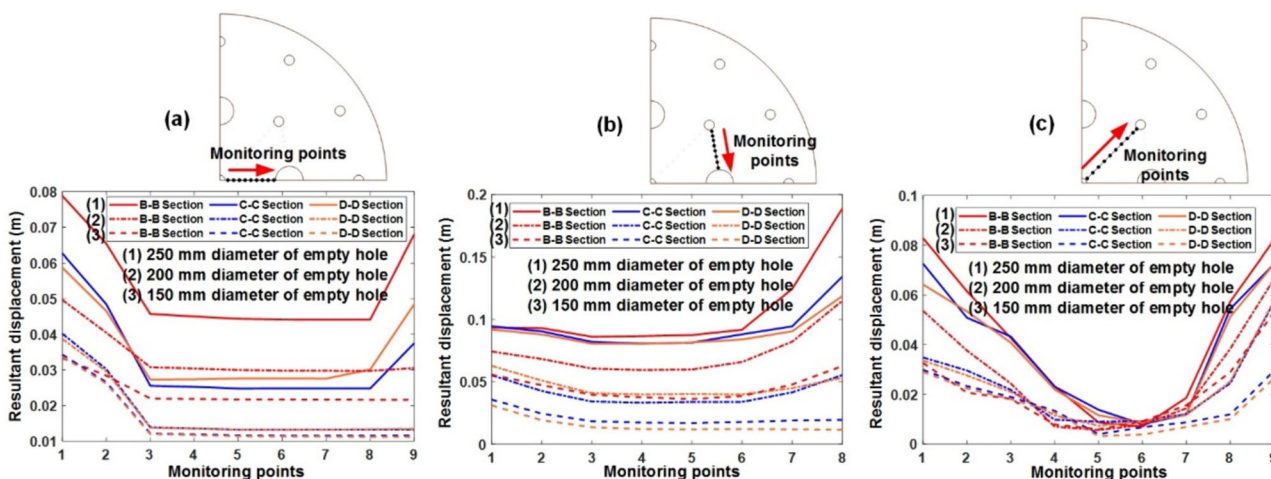


Fig. 14 Blast-induced peak resultant displacements along the connections of a the centric main borehole and empty holes, b the side main borehole and empty holes, and c the centric and side main boreholes in the cases with different diameters of empty holes

be found that the rock deformation near the empty holes along the connection of the centric main blasting borehole and empty holes in the B–B section is obviously increased in the case with 250 mm diameter of empty holes, while it is not significantly increased in the cases with 200 mm and 150 mm diameters of empty holes. The results further demonstrate that the bending-induced deformation of rock mass between main boreholes and empty holes is decreased with the decreased diameters of empty holes.

To investigate the effects of the diameters of empty holes on the rock fragmentation induced by the multi-long-hole blasting, the size distribution characteristics of rock fragments induced by the multi-long-hole blasting with different diameters of empty holes are obtained (see Fig. 15) by combining the analysis results of rock fragment sizes in multiple cross-sectional slices with different rock depths. The fitted results of size distributions of rock fragments based on Eq. (1) for these three cases are also given in Fig. 15. It can be seen that the ratios of small sizes of rock fragments induced by the multi-long-hole blasting are gradually decreased with the reduced diameters of empty holes. The reduction in the proportion of small sizes of rock fragments is more pronounced with the diameters of empty holes decreased from 250 to 200 mm than from 200 to 150 mm. The results show that increasing the diameter of empty holes to a certain level (e.g., 250 mm in this study) can improve rock fragmentation distribution under multi-long-hole blasting.

4.3 Effects of Spacing of Empty Hole and Main Borehole

To investigate the effect of spacings of the empty hole and main borehole on the performance of multi-long-hole blasting, the numerical models of rock mass subjected to multi-long-hole blasting with three different spacings (i.e., 0.5 m, 0.625 m, and 0.75 m) of empty holes and main boreholes are established in this section. Besides the spacings of the empty holes and main boreholes, other configurations of numerical models remain the same as those in Sect. 2.2.

Figure 16 shows the final blast-induced rock damage in the cases with different spacings of the empty holes and main boreholes. It can be found from the vertical view in Fig. 16 that the damage of rock mass in the main blasting area in the case with the spacing of 0.5 m is more severe than those in the other two cases. It is because the thicknesses of rock mass between the main borehole and empty holes are reduced with the reduced spacings, which thus favors the damage of rock mass in the main blasting area. However, the damage between the main boreholes and peripheral boreholes is not connected and aggregated well in the first case, while is effectively generated in the other two cases. In addition, it can be found from the cross-sectional views in Fig. 16 that with the increased spacings of the main boreholes and empty holes, although the damage range (e.g., the damage shown in the D–D section in Fig. 16) of rock mass in the main blasting areas increases, the undamaged rock mass in the main blasting is gradually increased. It is because the increased thickness of rock mass between the main boreholes and empty holes with the increased spacings increases the bending stiffness of rock mass and thus

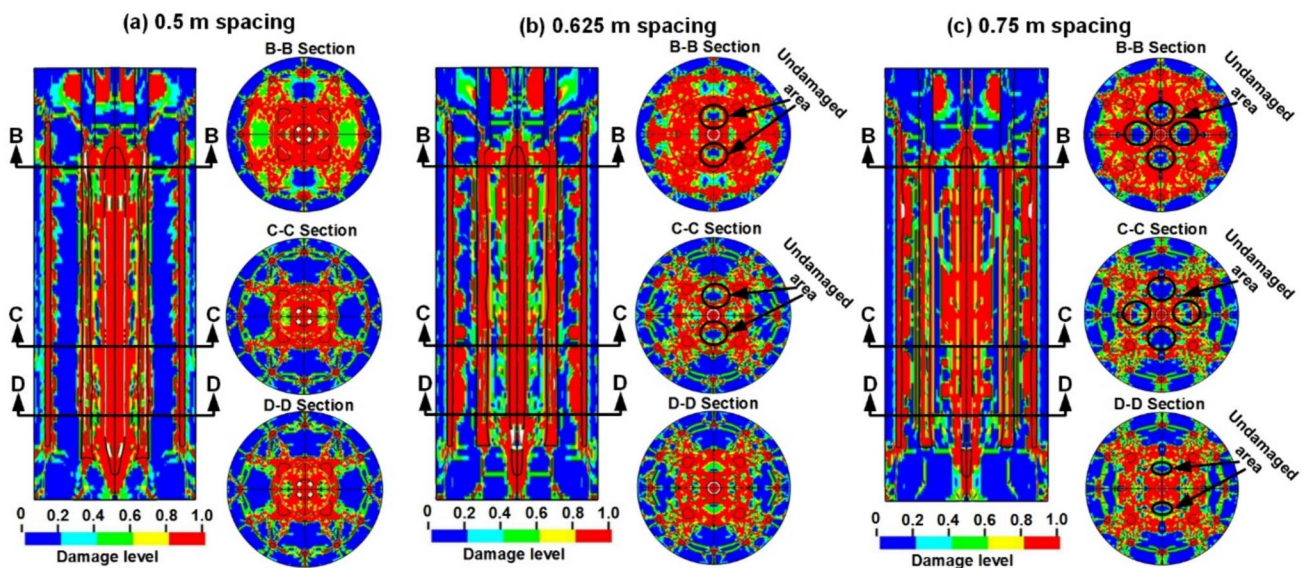


Fig. 16 Final damage of rock mass under multi-long-hole blasting with different spacings of empty holes and boreholes

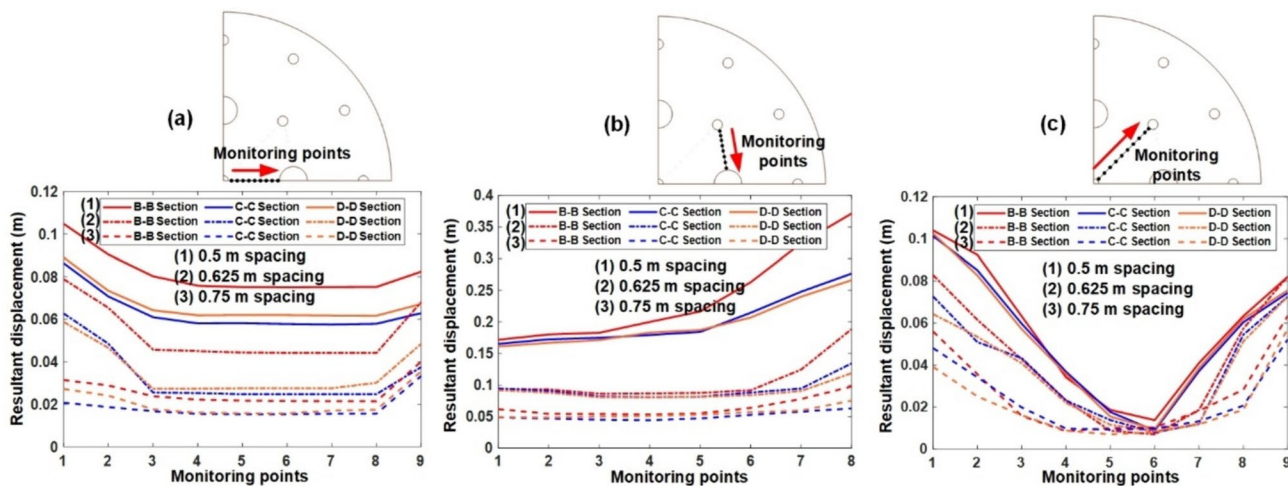


Fig. 17 Blast-induced peak resultant displacements along the connections of **a** the centric main borehole and empty holes, **b** the side main borehole and empty holes, and **c** the centric and side main boreholes in the cases with different spacings of empty holes and boreholes

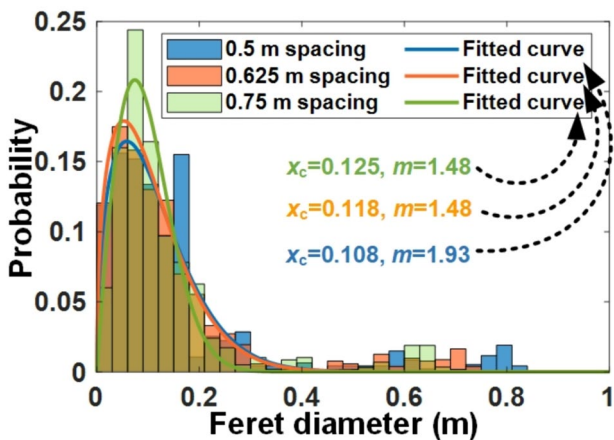


Fig. 18 Size distributions of blast-induced rock fragments in the cases with different spacings of empty holes and boreholes. Brown bars are the overlapping results of yellow and blue bars (Color figure online)

causes less bending-induced tensile damage of rock mass. The resultant displacements of rock mass in the main blasting areas shown in Fig. 17 further indicate that the bending-induced deformation of rock mass is reduced with the increased spacings of the main boreholes and empty holes. Based on the above results, it can be concluded that reducing the spacings of the main boreholes and empty holes can increase the damage levels of the main blasting areas but reduce the damage ranges of rock mass in the main blasting areas.

Figure 18 shows the size distributions of rock fragments induced by multi-long-hole blasting with different spacings of the main boreholes and empty holes. The fitted results of size distributions of blast-induced rock fragmentation based on

Eq. (1) are also given in Fig. 18. It can be seen that the ratios of small sizes (e.g., less than 90 mm) of rock fragments induced by multi-long-hole blasting increase with the increased spacings. It is because increasing the spacings of the main boreholes and empty holes can reduce the ratios of large rock fragments generated in the areas between the main blasting areas and peripheral holes, while the rock mass in the main blasting areas still can be well-broken with the spacings increased from 0.5 to 0.75 m. In addition, a significant increase in ratios of small sizes of rock fragments is achieved when the spacing is 0.75 m. The results demonstrate that increasing the spacings of the main boreholes and empty holes to a certain level can significantly improve rock fragmentation (i.e., decrease the ratios of large rock fragments).

5 Discussion

The results in Sect. 4 indicate that the configurations of empty holes significantly affect the damage ranges (i.e., shaft-forming ranges) and fragmentation of rock mass under multi-long hole blasting due to distinct ways of connections and aggregations of blast-induced rock damage under different configurations of empty holes. Therefore, it is essential to ensure appropriate configurations of empty holes for multi-long-hole blasting to achieve the expected damage and breakage of rock mass.

Combined with the results in Sect. 3, the damage of rock mass between the main boreholes and empty holes under blast loads can be approximately divided into three areas, i.e., the compressive damage around main boreholes, reflected tensile damage around empty holes, and combined shear and bending-induced tensile damage at the middle area, as illustrated in Fig. 19a. The formulas to determine

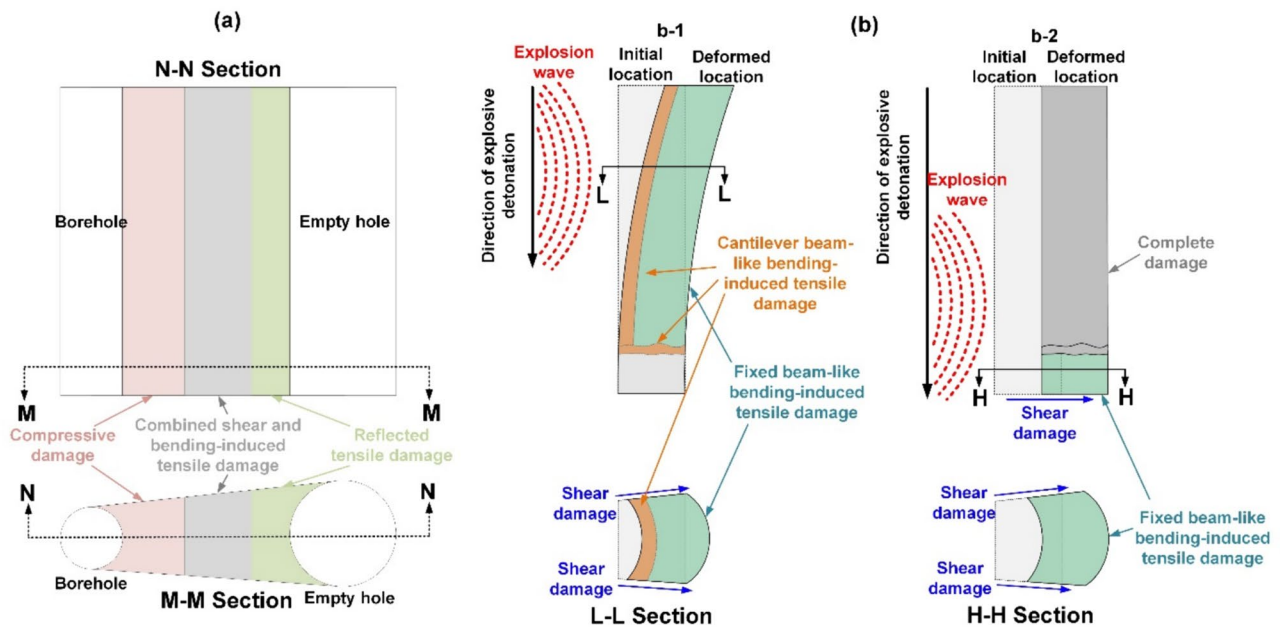


Fig. 19 Illustration of rock damage between boreholes and empty holes. **a** Damage area division and **b** mechanism of combined shear and bending-induced tensile damage in the middle area

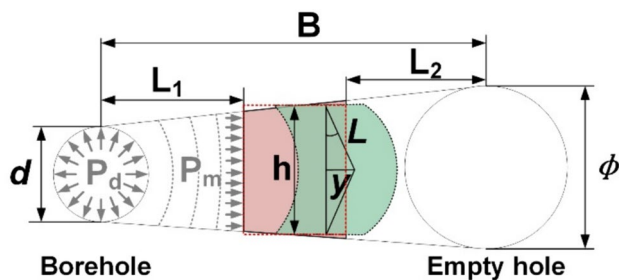


Fig. 20 Illustration for the calculation of the combined shear and bending-induced tensile damage in the middle area

the ranges of blast-induced compressive damage around the borehole and reflected tensile damage around the empty hole have been developed and documented in existing studies (Sun 2013; Zhang 2016). However, the formula for evaluating the combined shear and bending-induced tensile damage at the middle area has not yet been proposed. The section aims to develop the formulas to evaluate the combined shear and bending-induced tensile damage based on the results obtained in this study.

At the initial blasting stage, the upper rock mass in the area with the combined shear and bending-induced tensile damage experiences cantilever-beam-like bending-induced tensile damage due to the blast-induced axial bending deformation, fixed-beam-like bending-induced tensile damage due to the blast-induced deformation along the cross sections, and shear damage along the tangent of the borehole and empty hole due to the uncoordinated deformation

around the side tangents, as illustrated in Fig. 19b. With the downward detonation of explosives along the axial direction, the lower rock mass in this area is mainly destroyed under the fixed-beam-like bending-induced tensile damage, and the shear damage along the side tangents and bottom of the borehole and empty hole. The lower rock mass is more difficult to break than the upper rock due to the lack of cantilever-beam-like bending-induced tensile damage in the lower rock mass. Therefore, ensuring the effective damage of the lower rock mass in the middle area under blast loads is critical to develop reliable formulas for evaluating the combined shear and bending-induced tensile damage.

According to the damage modes and mechanism of the lower rock mass in the middle area, the tensile damage induced by the fixed-beam-like bending under blast loads is governed by the following equation:

$$\sigma_t f(\dot{\epsilon}_t) \leq E \cdot \epsilon_t = E \cdot \frac{2L - h}{h}, \tag{2}$$

where σ_t is the tensile strength of rock mass, $f(\dot{\epsilon}_t)$ is the dynamic increasing factor of tensile strength at the strain rate $\dot{\epsilon}_t$, E is the elastic modulus of rock mass, ϵ_t is the tensile strain of rock mass, h is the height of rectangular rock mass equivalent to trapezoidal rock mass (see Fig. 20), L is the half length of deformed rock mass. Based on the geometric relation, h and L can be obtained by Eqs. (3) and (4):

$$h = \frac{(B + L_1 - L_2)(\phi - d)}{2B} + d \tag{3}$$

$$L = \sqrt{\left(\frac{h}{2}\right)^2 + y^2}, \quad (4)$$

where B is the burden, i.e., the centric distance between the borehole and empty hole, ϕ and d are, respectively, the diameters of the empty hole and borehole, L_1 and L_2 are, respectively, the thicknesses of compressive damage around the borehole and reflected tensile damage around the empty hole, y is fixed-beam-like bending deflection and can be calculated by

$$y = \frac{P_m h^4}{384EI}, \quad (5)$$

where P_m is the pressure acting on the middle area, which can be determined based on the blast pressure acting on the borehole wall and the thickness of compressive damage. EI is the bending stiffness of rock mass in the middle area.

In addition, the shear damage of the lower rock mass in the middle area is governed by

$$\sigma_s f(\dot{\epsilon}_s) \leq G \cdot \epsilon_s = G \cdot \frac{\Delta L_s}{B - L_1 - L_2}, \quad (6)$$

where σ_s is the shear strength of rock mass, $f(\dot{\epsilon}_s)$ is the dynamic increasing factor of shear strength at the strain rate $\dot{\epsilon}_s$, G is the shear modulus of rock mass, ϵ_s is the shear strain of rock mass, ΔL_s is the shear deformation along the tangent of the borehole and empty hole or along the hole bottom, which can be determined based on shear force and shear stiffness, as given in Eqs. (7) and (8):

$$\text{Along the tangent : } \Delta L_s = \frac{P_m h}{2G \cdot (B - L_1 - L_2)} \quad (7)$$

$$\text{Along the hole bottom : } \Delta L_s = \frac{P_m}{2G \cdot (B - L_1 - L_2)} \quad (8)$$

According to Eqs. (2) and (6), the area with the combined shear and bending-induced tensile damage can be evaluated, which can be combined with existing formulas of compressive damage and reflected tensile damage to analytically derive the effective configurations of empty holes for multi-long-hole blasting.

6 Conclusion

The present study experimentally and numerically investigates the damage and fragmentation of rock mass under multi-long-hole blasting with large-diameter empty holes. The damage modes and mechanism of rock mass under this blasting are analysed and discussed. The effects of

configurations of empty holes on the performance of multi-long-hole blasting are also examined. The main conclusions are summarized as follows.

1. The rock mass under multi-long-hole blasting with large empty holes is subjected to compressive damage around boreholes, reflected tensile damage near empty holes, bending-induced tensile damage between empty holes and boreholes, and tensile damage between boreholes due to the superposition of stress waves, and shear damage along the tangent of empty holes and boreholes.
2. The empty holes can reduce the confined levels of blasted rock mass and thus facilitate rock damage and breakage levels under blast loads.
3. The depths of empty holes greatly influence the depth of effective damage of rock mass induced by multi-long-hole blasting (i.e., the shaft-forming depth in this study). The diameter of empty holes and the spacing between boreholes and empty holes can affect the blast-induced deformation levels of rock mass surrounded by empty holes due to different flexural rock stiffness with varied hole diameters and spacings.
4. Analytical formulas are developed to evaluate the combined shear and bending-induced tensile damage located between boreholes and empty holes. They can be combined with the existing calculation formulas of other types of damage to quantify the configurations of empty holes for multi-long-hole blasting.

Acknowledgements The authors acknowledge the financial support from the Key Science and Technology Project of Guangxi transportation industry.

Funding Open Access funding enabled and organized by CAUL and its Member Institutions. Funding was supported by Key Science and Technology Project of Guangxi transportation industry.

Data availability Data will be made available on request.

Declarations

Conflict of interest The authors declare that they have no known competing financial interests or personal relationships that could have appeared to influence the work reported in this paper.

Open Access This article is licensed under a Creative Commons Attribution 4.0 International License, which permits use, sharing, adaptation, distribution and reproduction in any medium or format, as long as you give appropriate credit to the original author(s) and the source, provide a link to the Creative Commons licence, and indicate if changes were made. The images or other third party material in this article are included in the article's Creative Commons licence, unless indicated otherwise in a credit line to the material. If material is not included in the article's Creative Commons licence and your intended use is not permitted by statutory regulation or exceeds the permitted use, you will need to obtain permission directly from the copyright holder. To view a copy of this licence, visit <http://creativecommons.org/licenses/by/4.0/>.

References

- Adhikari GR, Babu AR, Balachander R, Gupta RN (1999) On the application of rock mass quality for blasting in large underground chambers. *Tunn Undergr Space Technol* 14:367–375
- AyalaCarcedo F (2018) *Drilling and blasting of rocks*. Routledge, London
- Chandrakar S, Paul PS, Sawmliana C (2023) Long-hole raise blasting in a single shot: assessment of void ratio and delay time based on experimental tests. *Eng Struct* 275:115272
- Cheng R, Chen W, Hao H, Li J (2021a) A state-of-the-art review of road tunnel subjected to blast loads. *Tunn Undergr Space Technol* 112:103911
- Cheng R, Zhou Z, Chen W, Hao H (2021b) Effects of axial air deck on blast-induced ground vibration. *Rock Mech Rock Eng* 55:1037–1053
- Ding J, Yang J, Ye Z, Leng Z, Yao C, Zhou C (2023) Cut-blasting method selection and parameter optimization for rock masses under high in situ stress. *Int J Geomech* 23:04023211
- Himanshu VK, Mishra AK, Roy MP, Vishwakarma AK, Singh PK (2021) Numerical simulation based approach for assessment of blast induced deformation pattern in slot raise excavation. *Int J Rock Mech Min Sci* 144:104816
- Hudaverdi T, Kuzu C, Fısne A (2012) Investigation of the blast fragmentation using the mean fragment size and fragmentation index. *Int J Rock Mech Min Sci* 56:136–145
- Jong Y, Lee C-I, Jeon S, Cho Y-D, Shim D-S (2004) Performance assessment of the circular-cut blasting by numerical analysis. *Geosystem Eng* 7:75–82
- Konya CJ, Walter EJ (1991) *Rock blasting and overbreak control*. Administration, U.S.F.H., FHWA-HI-92-001
- Li X, Liu K, Yang J, Song R (2022) Numerical study on blast-induced fragmentation in deep rock mass. *Int J Impact Eng* 170:104367
- Liu K, Li Q, Wu C, Li X, Li J (2018) A study of cut blasting for one-step raise excavation based on numerical simulation and field blast tests. *Int J Rock Mech Min Sci* 109:91–104
- Mandal SK, Singh MM, Dasgupta S (2007) Two-dimensional theoretical model for design of burn-cut pattern. *Min Technol* 116:32–39
- Ouchterlony F, Sanchidrián JA (2019) A review of development of better prediction equations for blast fragmentation. *J Rock Mech Geotech Eng* 11:1094–1109
- Persson PA, Holmberg R, Lee J (2018) *Rock blasting and explosives engineering*. CRC Press, Boca Raton
- Roy MP, Paswan RK, Sarim MD, Kumar S, Jha R, Singh PK (2016) Rock fragmentation by blasting—a review. *J Mines Met Fuels* 64:424–431
- Sanchidrián JA, Segarra P, López LM (2007) Energy components in rock blasting. *Int J Rock Mech Min Sci* 44:130–147
- Sanchidrián JA, Castedo R, Lopez LM, Segarra P, Santos AP (2015) Determination of the JWL constants for ANFO and emulsion explosives from cylinder test data. *Cent Eur J Energetic Mater* 12:177–194
- Shapiro VY (1989) Efficiency of cut configuration in driving tunnels with a set of deep blast holes. *Sov Min Sci* 25:379–386
- Shi X, Xie C, Huo X, Qiu X, Wang Y (2023) Optimization of borehole layout in upwards medium-deep hole cut blasting. *Min Metall Explor* 40:1839–1848
- Sun C (2013) *Damage zone prediction for rock blasting*. Department of Mining Engineering, U.o.U.
- Thurley MJ (2011) Automated online measurement of limestone particle size distributions using 3D range data. *J Process Control* 21:254–262
- Xie LX, Lu WB, Zhang QB, Jiang QH, Chen M, Zhao J (2017) Analysis of damage mechanisms and optimization of cut blasting design under high in-situ stresses. *Tunn Undergr Space Technol* 66:19–33
- Yilmaz O (2023) Drilling and blasting designs for parallel hole cut and V-cut method in excavation of underground coal mine galleries. *Sci Rep* 13:2449
- Zare S, Bruland A (2006) Comparison of tunnel blast design models. *Tunn Undergr Space Technol* 21:533–541
- Zare S (2007) *Drill and blast tunnelling blast design*. REPORT 2A-05
- Zhang Z (2016) *Rock fracture and blasting: theory and applications*. Butterworth-Heinemann/Elsevier, Oxford, p 674
- Zhang H, Li T, Du Y, Zhu Q, Zhang X (2021) Theoretical and numerical investigation of deep-hole cut blasting based on cavity cutting and fragment throwing. *Tunn Undergr Space Technol* 111:103854
- Zhang Z-X, Sanchidrián JA, Ouchterlony F, Luukkanen S (2022) Reduction of fragment size from mining to mineral processing: a review. *Rock Mech Rock Eng* 56:747–778
- Zhang Z, Qiu X, Shi X, Luo Z, Chen H, Zong C (2023) Burden effects on rock fragmentation and damage, and stress wave attenuation in cut blasting of large-diameter long-hole stopes. *Rock Mech Rock Eng* 56(12):8657–8675
- Zhou Z, Cheng R, Cai X, Jia J, Wang W (2019) Comparison of presplit and smooth blasting methods for excavation of rock wells. *Shock Vib* 2019:3743028

Publisher's Note Springer Nature remains neutral with regard to jurisdictional claims in published maps and institutional affiliations.